Paper 67-4 has been designated as a Distinguished Paper at Display Week 2018. The full-length version of this paper appears in a Special Section of the *Journal of the Society for Information Display (JSID)* devoted to Display Week 2018 Distinguished Papers. This Special Section will be freely accessible until December 31, 2018 via:

http://onlinelibrary.wiley.com/page/journal/19383657/homepage/display_week_2018.htm

Authors that wish to refer to this work are advised to cite the full-length version by referring to its DOI:

https://doi.org/10.1002/jsid.655

5.8-inch QHD Flexible AMOLED Display with Enhanced Bendability of LTPS TFTs

Jaeseob Lee, Thanh Tien Nguyen, Joonwoo Bae, Gyoochul Jo, Yongsu Lee, Sunghoon Yang, Hyeyong Chu, Jinoh Kwag
Display Research Center, Samsung Display Co., LTD., Giheung-Gu, Youngin-Si, Gyeonggi-Do, Korea
Contact Author Email: jaeseob.lee@samsung.com

Abstract
By applying the curve-type TFT with longitudinal strain, TFT parameters do change little down to the 2R bending. The mobility variation range reduces down to 4% compared with 28% of the line-type channel with transverse strain. The smaller variation is preferred for a high quality display. We clarified that majority carrier's effective mass and scattering rate are dominant factors influencing the bended TFT's performance, which can be controlled by the strain orientation and channel shape. These understanding and improvement was embedded in the 5.8" flexible QHD AMOLED panel with multi edge curvature of Galaxy S8. Through this achievement, we made our flexible premium AMOLED panels more performable, reliable and highly productive in small R bending circumstance.

Author Keywords
Flexible AMOLED; LTPS TFTs; Uniaxial / Biaxial; Longitudinal / Transverse; Strain.

1. Introduction
In addition to AMOLED (active matrix organic light emitting diode) attractions such as vivid-color, free viewing angle, low power consumption, high contrast, fast response, and zero audible noise, flexibility-induced merits such as slim, rugged, light, user-friendly & free-style designed, flexible AMOLED display is the present and future promising display for mobile and TV applications. Samsung Display succeeded in bringing into worldwide use of multi-curvature flexible AMOLED in 2016, 2017 since introduction for the first time in the world in 2013, as shown in Fig. 1.

(a) (b)

Figure 1. Photographs of (a) Galaxy round of 5.7" FHD panel with 400R, 2013 (b) Galaxy S8 of 5.8" QHD+ panel with multi-curvature down to 3.8R, 2017.

The thin film transistor (TFT) technology for the flexible AMOLED has been oriented to integrate LTPS (low temperature polycrystalline Si) TFTs on the flexible substrate because polycrystalline silicon (poly-Si) TFT has a high mobility and stability required for AMOLED. These advantages are the most important reason why the poly-Si TFT technology is applied to the flexible AMOLED. It becomes an essential prerequisite to fabricate such a highly reliable and performable LTPS TFTs with robust bending properties for the flexible AMOLED panel. Therefore poly-Si TFT's bending characteristics must be deeply understood and engineered to be non-degenerated down to the small R (which means a bending radius, mm) such as 1~2R.

Electrical characteristics of the strained transistors were profoundly investigated in the single crystal Si MOSFETs. It was reported that the carrier mobility increases by the decrease of the scattering rate and effective mass of carriers when strain is applied [1~7]. For strained p-MOSFETs, it was observed that (I) biaxial tensile, (II) longitudinal uniaxial compressive and (III) biaxial tensile plus additional longitudinal uniaxial tensile strain increases the hole mobility. The mechanism is like that (I) the biaxial tensile strain mainly reduce the scattering rate by not only decreasing the acoustic scattering rate via altering the light and heavy hole band density of states but also decreasing the interband optical phonon scattering through light to heavy hole band splitting (ΔE), and (II) the longitudinal uniaxial compressive strain mainly reduce the conductivity effective mass by significant band warping. (III) Biaxial plus additive uniaxial tensile strain decreases the scattering rate more than the biaxial strain only, resulting in the more increment of hole mobility [8, 9].

In this paper we investigated the IV characteristics of the bended p-channel poly-Si TFTs and compared with that of the strained Si MOSFETs. Through these, we modeled the plausible mechanism influencing the bended LTPS TFTs. Besides we suggest the optimum arrangement of the strain orientation and channel shape for the minimization of the TFT parameter scattering in 2R bending. Through these fundamental understandings and improvement, we succeeded in making 5.8" flexible QHD+ AMOLED panel with multi-curvature of Galaxy S8 (Fig. 1(b)).

2. Experiments
Polymer film was prepared on glass with coating and thermal curing. Then, a conventional LTPS process sequence has been implemented to fabricate TFT backplane. The main TFT fabrication processes are as follows. First, a buffer layer was deposited to block impurities. Next, a 50 nm a-Si layer was deposited by plasma-enhanced chemical vapor deposition (PECVD). The a-Si film was irradiated with XeCl excimer laser beam (λ = 308 nm). A gate insulator (GI) was deposited using the PECVD. Gate metal was formed, and then followed by ion doping on the top poly-Si, using an ion doping system. Diffusion anneals were performed in nitrogen ambient by a conventional LTPS activation method. After a dielectric material for an interlayer was deposited, contact holes were patterned, followed by the deposition of source/drain metal and subsequent patterning to form electrodes. The EL layers were stacked under the base vacuum of about 10^{-6} torr in a thin-film evaporation coater. The OLED device structure consisted of hole injection layer (HIL), hole transport layer (HTL), RGB emitting layer (EML), hole blocking layer (HBL), electron transfer layer (ETL), electron injection layer (EIL), and transparent cathode. The

phosphorescent red, green, and fluorescent blue were used as emitting materials. Novel OLED structure with blue common layer (BCL) was applied to reduce blue patterning. When the panel fabrication was completed, the plastic layer was mechanically released by peeling off the plastic substrate from the rigid carrier.

3. Results

Fig. 2 shows the schematic diagram of the LTPS TFTs that are transverse or longitudinally strained, where the current are perpendicular or parallel with the applied strain, respectively [10~14]. For realization of an external strain, the samples are mounted in a custom-made cylindrical metal tube, as shown in Fig 3. The end of sample is fastened with the Kapton tape. The tensile and compressive strain direction and amounts are determined by the cylinder shape and radius.

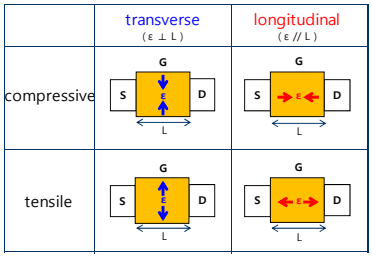

Figure 2. Schematic top view of transverse (perpendicular) and longitudinal (parallel) strain to the channel length. All applied strains are uniaxial.

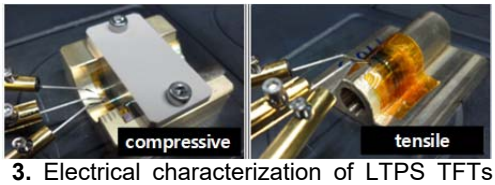

Figure 3. Electrical characterization of LTPS TFTs under compressive or tensile strain. Each cylindrical metal tube has various radiuses such as 2 to 7R (mm).

Fig. 4 shows photomicrographs of the line-, grid-, curve-type TFTs that have various ratio of perpendicular and parallel strain component with the applied external stress. Line-type TFT has a 100% of perpendicular strain to the current flow (ε⊥L) under bending parallel to the gate metal line. Whereas, grid-type TFT has a 75% perpendicular and 25% parallel strain, and curve-type TFT has a 60% perpendicular and 20% left-up and 20% right-up shear strain to the current flow under bending parallel to the gate metal line.

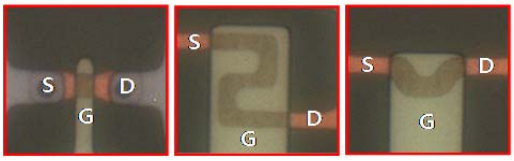

(a) line type (b) grid type (c) curve type

Figure 4. Photomicrographs of line-, grid- and curve- type transistors. TR size is (a) WxL=4x4, (b) 3.5x40 and (c) 3.5x17.6.

Fig. 5 shows the variation of the field effect mobility and driving voltage range of the p-channel LTPS TFTs with compressive and tensile strains of up to 0.47% (2R), where electrical characterization was done with 15 TRs in each condition. The strain orientation is such that the transverse (ε⊥L) means parallel to the gate line & perpendicular to the source-drain line and the longitudinal (ε∥L) means perpendicular to the gate line & parallel to the source-drain line. As seen in the figure, the normalized electrical responses change dramatically depending on the strain direction, orientation and TFT type. The biggest change is with the compressive-, transverse-strained line-type TFTs, where 16.2±4.5% increase of the field effect mobility and 1.6±4.5% decrease of the driving voltage range under the -0.47% of compressive strain (Fig. 5(a), blue line). Whereas the smallest change is in the tensile-, longitudinal-strained curve-type TFTs, where 0.3±0.6% increase of the mobility and 0.3±0.4% decrease of the DR range under the +0.47% of tensile strain (Fig. 5(c), red line). In general, the value shift and distribution range is huge in the transverse rather than longitudinal, the compressive rather than tensile strain, and the line-type rather than curve-type TFTs. This is clearly shown again in Fig. 6 and table 1.

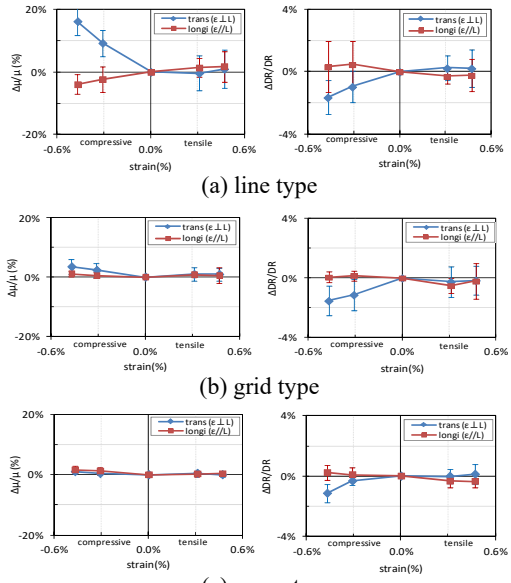

(a) line type

(b) grid type

(c) curve type

Figure 5. Normalized field effect mobility, driving voltage range variation under the transverse (perpendicular), longitudinal (parallel), compressive and tensile strain on the line-, grid-, and curve-type p-channel LTPS TFTs.

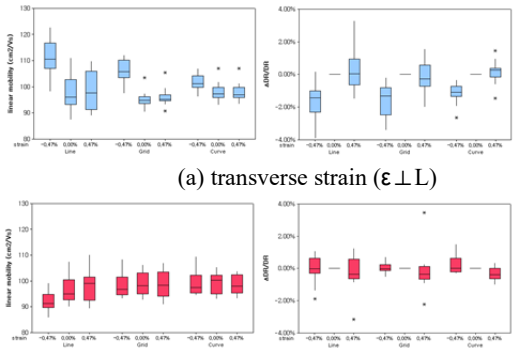

(a) transverse strain (ε⊥L)

(b) longitudinal strain (ε∥L)

Figure 6. Comparison of linear field effect mobility and normalized driving voltage range distribution in ±0.47% strained line-, grid-, curve-type TFTs in transverse (perpendicular) and longitudinal (parallel) strain orientation.

Table 1. Normalized field effect mobility, driving range, threshold voltage variation under the transverse (perpendicular), longitudinal (parallel), compressive, tensile strain on the line-, grid-, curve-type p-channel LTPS TFTs.

strain	type	transverse (ε⊥L)			longitudinal (ε//L)		
		Δμ/μ	ΔDR/DR	ΔVth/Vth	Δμ/μ	ΔDR/DR	ΔVth/Vth
Compressive (ε=-0.47%)	Line	16.2±4.5%	-1.6±1.1%	-3.2±2.1%	-4.0±3.1%	0.3±1.6%	-0.6±1.5%
	Grid	3.5±2.5%	-1.5±1.0%	-2.2±3.6%	1.1±1.0%	0.1±0.3%	-1.0±1.3%
	Curve	1.0±0.9%	-1.1±0.6%	-3.8±1.8%	1.6±1.3%	0.2±0.5%	-0.9±1.8%
Tensile (ε=+0.47%)	Line	1.0±6.1%	0.2±1.2%	-2.4±2.7%	1.8±4.9%	-0.2±1.0%	-2.5±2.3%
	Grid	0.9±2.1%	-0.2±1.0%	-3.2±2.4%	0.5±2.6%	-0.2±1.2%	-2.0±4.2%
	Curve	0.0±0.8%	0.1±0.7%	-2.8±2.0%	0.3±0.6%	-0.3±0.4%	-2.5±2.0%

The physics behind these strained p-channel poly-Si TFT behavior can be explained well. There were numerous reports about the strained c-Si MOSFET characteristics [1~7]. For strained p-channel MOSFETs, it was observed that (I) biaxial tensile, (II) longitudinal uniaxial compressive and (III) biaxial tensile plus additional longitudinal uniaxial tensile strain increases the hole mobility. The carrier mobility in strained silicon is determined like the following equations.

$$\mu_{eff} = \frac{q \cdot \tau}{m^*} \tag{1}$$

$$\mu_{eff} = q\left(\frac{\tau_{top}}{m^*_{top}} \cdot \frac{p_{top}}{p_{top}+p_{2nd}} + \frac{\tau_{2nd}}{m^*_{2nd}} \cdot \frac{p_{2nd}}{p_{top}+p_{2nd}}\right), \tag{2}$$

where τ is the scattering relaxation time (a.k.a. the time interval between the scattering events. Therefore, the scattering rate is proportional to 1/τ), m* is the conductivity effective mass of carriers. So both scattering rate and effective mass are responsible for the mobility change. It was proved that (I) the biaxial tensile strain mainly reduce the scattering rate by not only decreasing the acoustic scattering rate via altering the light and heavy hole band density of states but also decreasing the interband optical phonon scattering through light to heavy hole band splitting (ΔE). While it was proved that (II) the longitudinal uniaxial compressive strain mainly reduces the conductivity effective mass by significant band warping. Eq. (1) is a simplified formula and Eq. (2) is a complex one including the 1st and 2nd energy band contribution [1~7]. (III) Biaxial plus additive uniaxial tensile strain decreases the scattering rate more than the unique biaxial strain, resulting in the more increment of mobility [8, 9].

These quantum mechanics of the strained single crystal Si can be transported into the polycrystalline Si. Fig. 7 shows that polycrystalline Si has a weak but preferred crystal orientation of (100). In the EBSD (electron backscattering diffraction) pattern of the surface normal direction, the {001} orientation has a high portion in the surface orientation of (100), (110) and (111) [15, 16]. Also Raman spectrum show that the poly-Si film on plastic/glass substrate has a residual stress of 750~850 MPa biaxial tensile stress. The crystalline Si peak was red-shifted (to the lower frequency) with an amount of 3~3.5 cm^{-1} (compared with the 520cm^{-1} of non-strained c-Si) [17, 18]. This is due to the thermal misfit between Si and glass. The coefficients of thermal expansion (CTE) of Si and Glass are ~5 and ~3 ppm/℃ respectively. The detailed results are shown in Fig. 8 & table 2. The related formulas are eq. (3), (4). The external applied stress to poly-Si was calculated to be 496 to 752 MPa of uniaxial tensile or compressive, which was fixed by the metal cylinder radius and direction (table 3 and eq. (5)).

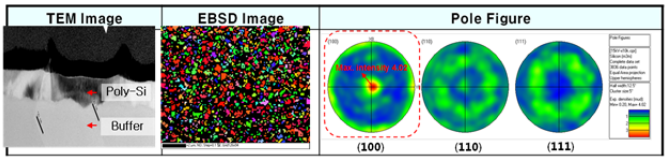

Figure 7. TEM cross-section image of poly Si film. The electron backscattering diffraction pattern shows that the film is mainly composed of (100)-oriented grains.

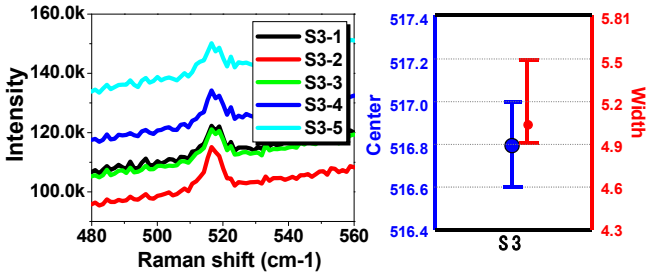

Figure 8. Raman spectra of poly-Si thin films on plastics/glass substrate. Peaks are shifted to lower frequency compared with the single crystalline Si wafer having no strain (reference, 520cm-1)

Table 2. The biaxial stress level of poly-Si film, determined by the wavenumber shift of the crystalline peak in Raman spectra.

ω(cm^{-1})	Δω(cm^{-1})	σ(MPa)	ε(%)
517.0	-3.0	750	0.47
516.6	-3.4	850	0.53

$$\Delta\varpi(cm^{-1}) = \varpi - \varpi_0 \tag{3}$$

$$\sigma(MPa) = -250 \times \Delta\varpi(cm^{-1}) \tag{4}$$

Table 3. The uniaxial stress induced by bending. The stress level was calculated by the Young's modulus definition.

R(mm)	ε(%)	E(GPa)	σ(MPa)
3	0.31	160	496
2	0.47	160	752

$$\sigma = E \cdot \varepsilon \tag{5}$$

To summarize, the poly-Si film under bended status suffers the biaxial tensile stress (750~850MPa) plus the additive uniaxial tensile or compressive stress (±496~752MPa). That means the poly-Si go through the maximum 1.3GPa tensile stress with longitudinal tensile of 2R bending and the minimum 0 ~ 100MPa tensile in longitudinal compressive of 2R. Also poly-Si has a preferred crystal orientation of (100) rather than the random orientation. This circumstance is similar with that of single crystal Si(c-Si) having a biaxial plus additive uniaxial strain. As p-channel MOSFET of c-Si has an increased mobility with the biaxial plus additive uniaxial tensile strain, our p-channel LTPS TFT also has an increased mobility with the longitudinal uniaxial tensile strain, which was clearly shown in the line-type transistor (fig. 5(a), red line). In case of transverse strain, the mobility increment vs. strain relationship changed the opposite, which is thought to be that the transverse strain (which is perpendicular to

the channel) influences the reverse effect to the longitudinal strain. Otherwise, grid- and curve-type transistors undergo little change of mobility during bending, which is thought to be due to the co-existence and effect-offset of the transverse and longitudinal strain (fig. 5 (b), (c)). Especially, the curve-type transistor showed little variation of mobility and driving voltage range down to 2R bending.

As far as the scattering is concerned to avoid the stain fault in display, the minimum change of TFT parameters is needed. From this viewpoint, the curve-type transistor with longitudinal strain is the best arrangement as a pixel driving TR (table 4). These curve-type transistors with longitudinal strain direction are embedded in the 5.8" flexible QHD+ AMOLED panel with multi-curvature of Galaxy S8.

Table 4. The comparison of the scattering range of parameters depending on the strain orientation and channel shape

Strain orientation / channel shape	Scattering range					
	3R			2R		
	Δμ	ΔDR	ΔV_{th}	Δμ	ΔDR	ΔV_{th}
Transverse strain / line type	9%	2%	3%	28%	4%	10%
Longitudinal strain / curve type	2%	1%	3%	4%	2%	5%

4. Conclusion

We proved that our p-channel LTPS TFTs on plastics did not degrade down to the 2R bending condition, which was due to the optimum combination of the channel shape and strain orientation, which means, the curve-type transistor with longitudinal strain applied. We clarified that p-channel LTPS TFT's performance variation on bending originates from majority carrier's scattering rate and effective mass change, which can be controlled by the strain orientation and channel shape. With this understandings and improvements, we fabricated the 5.8" flexible QHD+ AMOLED panel with multi-curvature of Galaxy S8. And we made our flexible premium AMOLED display more performable, reliable and highly productive in small R bending circumstance.

5. References

[1] S.E. Thompson, G. Sun, Y.S. Choi, T. Nishida, "Uniaxial-process-induced strained-Si: extending the CMOS roadmap," IEEE Trans. Elec. Dev. **53(5),** 1010-1020 (2006)

[2] S.E. Thompson, G. Sun, W.J. Lim, T. Nishida, "Key differences for process-induced uniaxial vs. substrate-induced biaxial stressed Si and Ge channel MOSFETs," IEDM 221-224 (2004)

[3] S.E. Thompson, M. Armstrong, C. Auth, etc, "A logic nanotechnology featuring strained-silicon," IEEE Elec, Dev. Let. **25(4),** 191-193 (2004)

[4] A. Chaudhry, S. Sangwan, J.N. Roy, "Mobility Modeling in a p-MOSFET under Uniaxial Stress," ELEKTROTEHNIŠKI VESTNIK (eng. ed.) **78(5)**, 298-303 (2011)

[5] Y. Sun, S.E. Thompson, T. Nishida, "Physics of strain effects in semiconductors and metal-oxide-semiconductor field-effect transistors," J. Appl. Phys. **101(10)**, 104503-1~22 (2007)

[6] M.L. Lee, E.A. Fitzgerald, M.T. Bulsara, M.T. Currie, A. Lochtefeld, "Strained Si, SiGe, and Ge channels for high-mobility metal-oxide-semiconductor field effect transistors," J. Appl. Phys. **97(1)**, 011101-1~26 (2005)

[7] S. Takagi, "Strained-Si CMOS technology," Advanced Mircoelectronics. **27**, 1-19 (2007)

[8] Z. Shuo, G. Lei, W. Jing, X. Jun, L. Zhihong, "Impacts of additive uniaxial strain on hole mobility in bulk Si and strained-Si p-MOSFETs," J. Semiconductors. **30(10)**, 104001-1~6 (2009)

[9] O. Weber, T. Irisawa, T. Numata, M. Harada, etc, "Examination of additive mobility enhancements for uniaxial stress combined with biaxially strained Si, biaxially strained SiGe and Ge channel MOSFETs," IEDM 719-722 (2007)

[10] P. Servati, A. Nathan, "Functional pixel circuits for elastic AMOLED displays," Proceedings of IEEE **93(7)**, 1257-1264 (2005)

[11] H. Irie, K. Kita, K. Kyuno, A. Toriumi, "In-Plane mobility anisotropy and universality under uni-axial strains in n- and p-MOS inversion layers on (l00), (110), and (111) Si," IEDM 225-228 (2004)

[12] K. Shimizu, T. Saraya, T. Hiramoto, "Physical understandings of Si (110) hole mobility in ultra-thin body pFETs by <110> and <111> uniaxial compressive strain," IEDM 473-476 (2009)

[13] K. Uchida, T. Krishnamohan, K.C. Saraswat, Y. Nishi, "Physical mechanism of electron miblity enhancement in uniaxial stressed MOSFETs and impact of uniaxial stress engineering in ballistic regime," IEDM 129-132 (2005)

[14] C.F.Huang, Y.J.Yang, C.Y.Peng, F.Yuan, C.W.Liu, "Mechanical strain effect of n-channel polycrystalline silicon thin-film transistors," Appl. Phys. Lett. **89(10)**, 103502-1~3 (2006)

[15] K. Kitahara, T. Ishii, J. Suzuki, T. Bessyo, N. Watanabe, "Characterization of defects and stress in polycrystalline silicon thin films on glass substrates by Raman microscopy," Int. J. of Spectroscopy, 632139-1~14 (2011)

[16] K. Kitahara, A. Hara, "Oriented lateral growth and defects in polycrystalline-silicon thin films on glass substrates," Crystallization - Science and Technology, Chap.19, 507-534 (2012)

[17] R.C. Teixeira, I. Doi, M.B.P. Zakia, J.A. Diniz, J.W. Swart, "Micro-Raman stress characterization of polycrystalline silicon films grown at high temperature," Mat. Sci. & Eng. B, **112(2~3)**, 160-164 (2004)

[18] C. Zhao, M. Li, M. Yin, Z. Liu, "Micro-Raman spectroscopy analysis of residual stress in polysilicon MEMS resonators" IEEE Int. Conf. on NEMS, 570-573 (2013)